Analytical Solution of Time Periodic Electroosmotic Flows: Analogies to Stokes' Second Problem

Prashanta Dutta[†] and Ali Beskok*,[‡]

Microfluidics Laboratory, Mechanical Engineering Department, Texas A&M University, College Station, Texas, 77843-3123, and School of Mechanical and Materials Engineering, Washington State University, Pullman, Washington 99164-2920

Analytical solutions of time periodic electroosmotic flows in two-dimensional straight channels are obtained as a function of a nondimensional parameter κ, which is based on the electric double-layer (EDL) thickness, kinematic viscosity, and frequency of the externally applied electric field. A parametric study as a function of κ reveals interesting physics, ranging from oscillatory "pluglike" flows to cases analogous to the oscillating flat plate in a semi-infinite flow domain (Stokes' second problem). The latter case differs from the Stokes' second solution within the EDL, since the flow is driven with an oscillatory electric field rather than an oscillating plate. The analogous case of plate oscillating with the Helmholtz−Smoluchowski velocity matches our analytical solution in the bulk flow region. This indicates that the instantaneous Helmholtz−Smoluchowski velocity is the appropriate electroosmotic slip condition even for high-frequency excitations. The velocity profiles for large κ values show inflection points very near the walls with localized vorticity extrema that are stronger than the Stokes layers. This have the potential to result in low Reynolds number flow instabilities. It is also shown that, unlike the steady pure electroosmotic flows, the bulk flow region of time periodic electroosmotic flows are rotational when the diffusion length scales are comparable to and less than the half channel height.

Electroosmosis is one of the major electrokinetic phenomena in which ionized liquid flows with respect to a charged surface in the presence of an external electric field. Although this phenomenon was first observed experimentally in the early nineteenth century, only recently has it received considerable attention from engineers and chemists due to the emergence of microfluidic devices. The pressure-building ability of electroosmosis made it very suitable as a pumping mechanism in microchannel geometries for electronic cooling[1] and bioanalytical systems.[2,3]

Time periodic electroosmotic flow is also known as A/C electroosmosis, and it is driven by an alternating electric field. Although time periodic electroosmotic flow has potential in biotechnology and separation science, it has been addressed in only a relatively few publications. For example, Dose and Guiochon reported numerical results for impulsively started electroosmotic flow,[4] and Soderman and Jonsson published an analytical work on starting problems of electroosmotic flows for a number of geometries including the flow over a flat plate and two-dimensional microchannel and microtube flows.[5] Green et al. investigated A/C electroosmosis on planner microelectrodes using steady and unsteady electric fields.[6] In a later study, they analyzed the same problem based on the linearized Debye layer theory.[7] Most recently, Barragan and Bauza experimentally studied the effects of a sinusoidally alternating electric field, superimposed onto a steady electroosmotic flow.[8]

Microscale combustion and power generation applications, as well as the "laboratory on a microchip" devices require development of reliable micromixers. Mixing in microfluidic systems is difficult due to the negligible inertial effects. Also, small molecular diffusion coefficients require longer convective/diffusive mixing length, time scales, or both. Moreover, microstirrers with moving components are usually difficult to build, and they are prone to mechanical failure. Currently, several ideas including peristaltic membrane motion and chaotic advection are being utilized to develop various micromixers.[9] Most recently, Oddy et al. have utilized pulsating electrostatic flows to promote and enhance mixing for low Reynolds number flows[10] (*Re* > 0.1) and built a micromixer that is capable of stirring two fluid streams continuously or intermittently.[11] Motivated by the potential of pulsating flows in promoting mixing, we study here the time periodic electroosmotic flows in straight microchannels by changing the

* Corresponding author: (e-mail) abeskok@mengr.tamu.edu; (phone) (979) 862-1073.
† Washington State University.
‡ Texas A&M University.

(1) Chen, C. H.; Zeng, S.; Mikkelsen, J. C.; Santiago, J. G. *Proc. ASME* **2000,** *MEMS 1,* 523−528.
(2) Chang, H. T.; Chen, H. S.; Hsieh, M. M.; Tseng, W. L. *Rev. Anal. Chem.* **2000,** *19* (1), 45−74.
(3) Anderson, G. P.; King, K. D.; Cuttiono, D. S.; Whelan, J. P.; Ligler, F. S.; MacKrell, J. F.; Bovais, C. S.; Indyke, D. K.; Foch, R. J. *Field Anal. Chem. Technol.* **1999,** *3* (4−5), 307−314.
(4) Dose, E. V.; Guiochon, G. *J. Chromatogr.* **1993,** *652,* 263−275.
(5) Soderman, O.; Jonsson, B. *J. Chem. Phys.* **1996,** *105,* 10300−10311.
(6) Green, N. G.; Ramos, A.; Gonzalez, A.; Morgan H.; Castellanos A. *Phys. Rev. E* **2000,** *61* (4), 4011−4018.
(7) Gonzalez, A.; Ramos, A.; Green, N. G.; Castellanos, A. *Phys. Rev. E* **2000,** *61* (4), 4019−4028.
(8) Barragan, V. M.; Bauza, C. R. *J. Colloid Interface Sci.* **2000,** *230,* 359−366.
(9) Yi, M.; Bau, H. H.; Hu, H. *Proc. ASME* **2000,** *MEMS 1,* 367−374.
(10) Oddy, M. H.; Santiago, J. G.; Mikkelsen, J. C. *Anal. Chem.,* submitted.
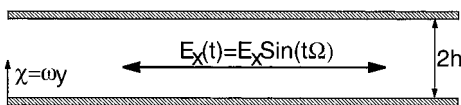(11) Oddy, M. H.; Mikkelsen, J. C.; Santiago, J. G. *Proc. ASME,* in press.

Figure 1. Schematic view of time periodic electroosmotic flow in a two-dimensional straight channel. Here Ω is the frequency of the external electric field and ω is the Debye–Hückel parameter.

Table 1. Variation of the Nondimensional Parameter κ as a Function of the EDL Thickness λ, Ion Concentration n_o, and Frequency of the Electric Field Ω[a]

ν (m²/s)	n_o (M)	λ (nm)	Ω (Hz)	κ
1.0×10^{-6}	1.0×10^{-4b}	30	1.0×10^3	0.001
			1.0×10^4	0.003
			1.0×10^5	0.010
1.0×10^{-6}	1.0×10^{-5b}	100	1.0×10^3	0.003
			1.0×10^4	0.010
			1.0×10^5	0.032
1.0×10^{-6}	1.0×10^{-6c}	320	1.0×10^3	0.010
			1.0×10^4	0.032
			1.0×10^5	0.100

[a] Here the frequencies are selected from the experimental work of Green at el.[6] [b]The ion concentrations are selected from Hunter.[12] [c]The ion concentrations are selected from Macounova et al.[13]

polarity of the externally imposed electric field. A schematic view of the geometry is shown in Figure 1. Here the time periodic electroosmotic forces act on the fluid as an alternating pulse. Typical values of the excitation frequency and the buffer concentration considered in this study are presented in Table 1. The data are based on various experimental conditions presented by Hunter,[12] Macounova et al.,[13] and Green et al.[6]

ANALYSIS OF TIME PERIODIC ELECTROOSMOTIC FLOWS

The motion of ionized, incompressible fluid with electroosmotic body forces are governed by the incompressible Navier–Stokes equations:

$$\rho_f\left(\frac{\partial \vec{V}}{\partial t} + (\vec{V}\cdot\nabla)\vec{V}\right) = -\nabla P + \mu\nabla^2\vec{V} + \rho_e\vec{E} \qquad (1)$$

where P is the pressure, ρ_f is the fluid density, μ is the dynamic viscosity, and $\vec{V} = (u, v)$ is a divergence-free velocity field ($\nabla\cdot\vec{V} = 0$) subject to the no-slip boundary conditions on the walls. The last term on the right-hand side indicates the electroosmotic body forces, where ρ_e is the electric charge density, and $\vec{E}$ is the externally applied electric field. Our analytical solution assumes *fully developed straight channel flow*. Therefore, the inertial terms in the Navier–Stokes equations are neglected. This results in the unsteady Stokes equations that are linear in velocity and, hence, allow solution using the superposition principle. Linearity of the equations allowed us to solve for the pressure and electroosmotically driven flows separately and combine the solution for mixed electroosmotic/pressure-driven flows under a unidirectional elec-

tric field.[14] In general, the electroosmotic body force term can exhibit various forms depending on the externally applied electric field. In this paper, we consider sinisoidally driven time periodic "pure electroosmotic flows" in the absence of pressure gradients. Under these conditions, we obtain

$$\rho_f\frac{\partial u}{\partial t} = \mu\frac{\partial^2 u}{\partial y^2} + \rho_e E_x \sin(\Omega\, t) \qquad (2)$$

where E_x is the magnitude and Ω is the frequency of the unsteady external electric field $\vec{E}$. We note here that due to the straight channel geometry the cross-stream velocity and electric field components are zero, and eq 2 is used to determine the streamwise velocity component due to the time-periodic electric field.

The electric charge density ρ_e in eq 2 can be expressed as

$$\rho_e = -2n_o ez \sinh\left(\frac{ez\psi}{k_B T}\right) = -2n_o ez \sinh(\alpha\psi^*) \qquad (3)$$

where n_o is the average number of positive or negative ions in the buffer, e is the electron charge, z is the valance, k_B is the Boltzmann constant, and T is the absolute temperature. In eq 3, $\psi^* = \psi/\zeta$ is the electroosmotic potential normalized with the zeta potential ζ, and α is the ionic energy parameter

$$\alpha = ez\zeta/k_B T$$

where $\zeta = 25.4$ mV at $T = 300$ K corresponds to $\alpha = 1$. Solution for the electroosmotic potential ψ is obtained from the Poisson–Boltzmann equation

$$\nabla^2\psi = -\rho_e/\epsilon$$

where ϵ is the permittivity. In this particular analysis, we assume that ψ is not affected by the time fluctuations of the external electric field, which can be justified by analysis of the ion conservation equation in two-dimensional straight channels.[15] In general, it is difficult to obtain a closed form analytical solution for the electroosmotic potential. Burgreen and Nakache[16] were able to obtain a solution of the Poisson–Boltzmann equation in a channel in terms of a first-kind elliptic integral for finite electric double-layer (EDL) thickness. Our analysis is valid for the cases where the EDL thickness is smaller than the channel half-height. Therefore, the electroosmotic potential distributions from the two walls do not interact with each other. In ref 14, we quantified this condition by defining an "effective EDL thickness" ($\delta_{99}\lambda$) as the distance from the wall, where the normalized electroosmotic potential reaches to 1% of its base value. In our definition, the effective EDL thickness (δ_{99}) is a function of the ionic energy parameter α. For example, the effective EDL thickness for $\alpha = 5$ is $\delta_{99} = 4.217\lambda$, where λ is an estimate of the electric double-layer thickness based on the Debye–Hückel parameter obtained

(12) Hunter, R. J. *Zeta Potential in Colloid Science: Principles and Applications*; Academic Press: New York, 1981.
(13) Macounova, K.; Cabrera, C. R.; Holl, M. R.; Yager, P. *Anal. Chem.* **2000**, *72*, 3745–3751.

(14) Dutta, P.; Beskok, A. *Anal. Chem.* **2001**, *73*, 1979–1986.
(15) Dutta, P. Ph.D. Dissertation, Texas A&M University, College Station, TX, 2001.
(16) Burgreen, D.; Nakache, F. R. *J. Phys. Chem.* **1964**, *68*, 1084–1091.

by

$$\omega = \frac{1}{\lambda} = \sqrt{\frac{8\pi n_o e^2 z^2}{D k_B T}}$$

Considering the exponential decay of the electroosmotic potential away from the walls, the top and bottom walls do not interact with each other if the channel half-height h is larger than 10λ (or $\omega h \geq 10$). For most microfluidic applications, λ is in the order of 10−100 nm, which is much smaller than a typical microchannel height. Under these conditions, the electroosmotic potential reaches zero in the channel center and the electroosmotic potential distribution can be written as a function of the distance from the wall ($\chi = y/\lambda$) as[12,14]

$$\psi^* = \frac{4}{\alpha} \tanh^{-1}\left[\tanh\left(\frac{\alpha}{4}\right)\exp(-\chi)\right] \qquad (4)$$

Using the definition of the Debye−Hückel parameter (ω), we can rewrite the electroosmotic body force on the fluid in the following form:

$$-2n_o ez E_x \sin \Omega t = \frac{\omega^2 \mu u_{HS}}{\alpha}\sin\Omega t \qquad (5)$$

where $u_{HS} = -\epsilon\zeta E_x/\mu$ is the Helmholtz−Smoluchowski velocity. Using these, eq 2 can be written as

$$\rho_f \frac{\partial u}{\partial t} = \mu \frac{\partial^2 u}{\partial y^2} + \frac{\omega^2 \mu u_{HS}}{\alpha}\sinh(\alpha\psi^*)\sin(\Omega t) \qquad (6)$$

We are interested in the solution of the above equation under no-slip and symmetry boundary conditions on the wall and the channel center, respectively. Nondimensionalization of eq 6 using characteristic time ($1/\Omega$) and length (λ) scales results in the following equation

$$\rho_f u_{HS}\Omega \frac{\partial U}{\partial\theta} = \mu u_{HS}\omega^2\left[\frac{\partial^2 U}{\partial\chi^2} + \frac{\sin(\theta)}{\alpha}\sinh(\alpha\psi^*)\right] \qquad (7)$$

where $\theta = \Omega t$ is the nondimensional time, $\chi = y/\lambda$ is the nondimensional distance, and $U = u/u_{HS}$ is the nondimensional velocity. Rearranging the dimensional components in eq 7 results in the following equation

$$\frac{\partial U}{\partial\theta} = \frac{1}{\kappa^2}\left[\frac{\partial^2 U}{\partial\chi^2} + \frac{\sin(\theta)}{\alpha}\sinh(\alpha\psi^*)\right] \qquad (8)$$

where $\kappa = (\Omega\lambda^2/\nu)^{1/2}$ is a normalized parameter that is a function of the Debye length (λ), the kinematic viscosity, and the electric field excitation frequency. The parameter κ can be interpreted as the ratio of the Debye length to a diffusion length scale (l_D), based on the kinematic viscosity and the excitation frequency. The diffusion length scale can be estimated from the unsteady Stokes equations using dimensional analysis as $l_D \simeq (\nu/\Omega)^{1/2}$. Hence, the diffusion length scale is related to the Debye length and κ in

the following form:

$$l_D \simeq \lambda/\kappa$$

Now we seek time-periodic solution of eq 8 by decomposing the velocity $U(\chi, \theta)$ into the space-dependent ($F(\chi)$) and time-dependent ($G(\theta)$) terms in the following form:

$$U(\chi, \theta) = F(\chi)\cdot G(\theta) = \text{Im}[\exp(i\theta)F(\chi)] \qquad (9)$$

where $\sin(\theta)$ is written as the imaginary part of $exp(i\theta)$ ($i = -1^{1/2}$). Therefore we will seek the *imaginary component of the final solution.*

Using the separation of variables principle, the time derivative of $U(\chi, \theta)$ can be expressed as

$$\frac{\partial U}{\partial\theta} = i\exp(i\theta)F(\chi)$$

and the second space derivative as

$$\frac{\partial^2 U}{\partial\chi^2} = exp(i\theta)\frac{d^2 F}{d\chi^2}$$

Hence eq 8 becomes

$$i\exp(i\theta)F(\chi) = \frac{\exp(i\theta)}{\kappa^2}\left[\frac{d^2 F}{d\chi^2} + \frac{\sinh(\alpha\psi^*)}{\alpha}\right] \qquad (10)$$

Since $\exp(i\theta)$ cannot be zero at all times, the spatial governing equation becomes

$$\frac{d^2 F(\chi)}{d\chi^2} - i\kappa^2 F(\chi) = -\frac{\sinh(\alpha\psi^*)}{\alpha} \qquad (11)$$

The complimentary function of the above differential equation can be written as

$$\text{CF} = A\exp(\sqrt{i}\kappa\chi) + B\exp(-\sqrt{i}\kappa\chi) \qquad (12)$$

where A and B are the coefficients of the homogeneous solution and they depend on the parameter κ. In the following section, we will briefly discuss the procedure of finding the constants A and B.

The particular integral of eq 11 can be obtained as

$$\text{PI} = \frac{1}{2\kappa\alpha\sqrt{i}}[\exp(-\sqrt{i}\kappa\chi)\int_0^\chi \exp(\sqrt{i}\kappa\chi)\sinh(\alpha\psi^*)\,d\chi]$$
$$- \frac{1}{2\kappa\alpha\sqrt{i}}[\exp(\sqrt{i}\kappa\chi)\int_0^\chi \exp(-\sqrt{i}\kappa\chi)\sinh(\alpha\psi^*)\,d\chi] \qquad (13)$$

Therefore, the spatial variation of velocity F can be expressed as

$$F(\chi) = A \exp(\sqrt{i\kappa}\chi) + B \exp(-\sqrt{i\kappa}\chi)$$

$$+ \frac{1}{2\kappa\alpha\sqrt{i}}[\exp(-\sqrt{i\kappa}\chi)\int_0^\chi \exp(\sqrt{i\kappa}\chi)\ \sinh(\alpha\psi^*)\ d\chi]$$

$$- \frac{1}{2\kappa\alpha\sqrt{i}}[\exp(\sqrt{i\kappa}\chi)\int_0^\chi \exp(-\sqrt{i\kappa}\chi)\ \sinh(\alpha\psi^*)\ d\chi] \quad (14)$$

and the velocity for time periodic electroosmotic flow becomes

$$U(\chi, \theta) =$$

$$\mathrm{Im}\Big\{\exp(i\theta)\ A\ \exp(\sqrt{i\kappa}\chi) + \exp(i\theta)\ B\ \exp(-\sqrt{i\kappa}\chi)$$

$$+ \frac{\exp(i\theta)}{2\kappa\alpha\sqrt{i}}[\exp(-\sqrt{i\kappa}\chi)\int_0^\chi \exp(\sqrt{i\kappa}\chi)\ \sinh(\alpha\psi^*)\ d\chi]$$

$$- \frac{\exp(i\theta)}{2\kappa\alpha\sqrt{i}}[\exp(\sqrt{i\kappa}\chi)\int_0^\chi \exp(-\sqrt{i\kappa}\chi)\ \sinh(\alpha\psi^*)\ d\chi]\Big\}$$

$$(15)$$

COEFFICIENTS OF THE HOMOGENEOUS SOLUTION

The values of constants A and B are found by using the boundary conditions. The no-slip condition on the channel wall requires $F(\chi = 0) = 0$. Therefore,

$$A = -B \quad (16)$$

The symmetry boundary condition at the channel center results in the following[15]

$$A = -B = \frac{1}{4\sqrt{i\kappa}\alpha\ \cosh(\sqrt{i\kappa}\chi)}[\exp(-\sqrt{i\kappa}\chi)$$

$$\int_0^\infty \exp(\sqrt{i\kappa}\chi)\ \sinh(\alpha\psi^*)\ d\chi]$$

$$+ \frac{1}{4\sqrt{i\kappa}\alpha\ \cosh(\sqrt{i\kappa}\chi)}[\exp(\sqrt{i\kappa}\chi)\int_0^\infty \exp(-\sqrt{i\kappa}\chi)\ \sinh$$

$$(\alpha\psi^*)\ d\chi] \quad (17)$$

The values of the constants A and B, as well as the particular solution presented in eq 13, are obtained by using a Romberg integration technique[17] based on the trapezoidal rule. In the Romberg integration technique, the numerical error can be reduced to a certain prescribed tolerance level by successive Taylor series expansions. The values of the constants A and B are listed in Table 2 as a function of κ and α. Here we must emphasize that the upper limit of integration in eq 17 is extended to $\chi \rightarrow \infty$ without loss of generality. This is justified because $\sinh(\alpha\psi^*) \rightarrow 0$, when $\chi \geq 10$. Therefore, the contributions for these integrals for $\chi \geq 10$ are negligible, and the channel center location can be treated as if it is at $\chi \rightarrow \infty$, as long as the half channel height is larger than 10λ.

DISCUSSION OF RESULTS

The time-periodic velocity distribution across the channel for three different κ values are shown in Figure 2 at time $\theta = \pi/2$.
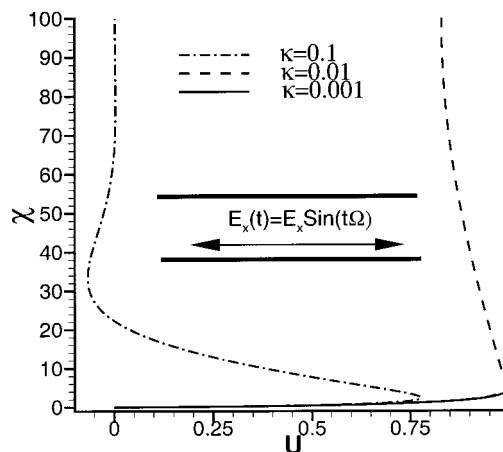
(17) Chapra, S. C.; Canale, R. P. *Numerical Methods for Engineers*; McGraw-Hill: New York, 1988.

Figure 2. Velocity distribution of time-periodic electroosmotic flow for various values of κ at time $\theta = \pi/2$. Here, the ionic energy parameter α = 5.

Table 2. Values of the Coefficients A and B as a Function of κ and the Ionic Energy Parameter

κ	α	A	B
0.1	1	$3.2193 - 3.6544i$	$-3.2193 + 3.6544i$
	3	$4.5500 - 4.9912i$	$-4.5500 + 4.9912i$
	5	$8.0828 - 8.5328i$	$-8.0828 + 8.5328i$
	7	$16.2326 - 16.6910i$	$-16.2326 + 16.6910i$
0.01	1	$36.4360 - 37.0551i$	$-36.4360 + 37.0551i$
	3	$49.7763 - 50.3961i$	$-49.7763 + 50.3961i$
	5	$85.1510 - 85.7718i$	$-85.1510 + 85.7718i$
	7	$166.6935 - 167.3152i$	$-166.6935 + 167.3152i$
0.001	1	$368.435 - 368.505i$	$-368.435 + 368.505i$
	3	$501.841 - 501.911i$	$-501.841 + 501.911i$
	5	$855.593 - 855.663i$	$-855.593 + 855.663i$
	7	$1671.023 - 1671.093i$	$-1671.023 + 1671.093i$

These results are obtained for a channel half-height $h = 100\lambda$. Using the estimated Debye length from Table 1, the typical channel half-heights correspond to 3, 10, and 32 μm, depending on the buffer concentration (n_0). Since the electroosmotic forces are confined within the EDL, the dynamics of fluid motion in the bulk of the channel is mostly determined by an unsteady diffusion process. Therefore, the magnitude of the channel half-height (h) relative to the diffusion length scale (l_D) plays an important role in determining the dynamics of the bulk flow region. For the $\kappa = 0.001$ case, the diffusion length scale ($l_D = 1000\lambda$) is an order of magnitude larger than the channel half-height (100λ). This results in a quasi-steady velocity distribution that resembles the "plug velocity" obtained in steady electroosmotic flows, as shown in Figure 2. On the other hand, for $\kappa = 0.01$, the channel half-height and the diffusion length scales are the same order of magnitude, and the bulk flow velocity deviates from the plug profile. For $\kappa = 0.1$, the velocity becomes practically zero in the channel center at any time, as shown in Figure 3. For a fixed channel dimension and buffer solution (i.e., fixed n_0 and ν), the values of κ directly depend on the frequency of the externally applied electric field. Therefore, $\kappa = 0.1$ corresponds to an electric field frequency of 100 kHz for a Debye length of 320 nm. It is possible to obtain this frequency by electronic switching, as demonstrated by Green et al.[6]

For the $\kappa = 0.01$ case, there is *vorticity* in the *entire* bulk flow region (See Figure 2). The vorticity is defined as the curl of the
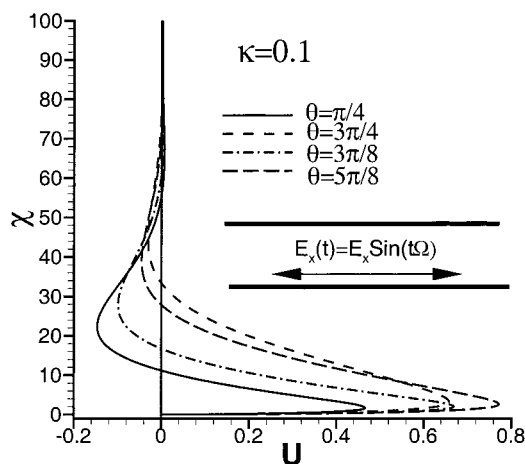
Figure 3. Velocity distribution for time-periodic electroosmotic flows at different times. Here, $\kappa = 0.1$ and the ionic energy parameter $\alpha = 5.0$.
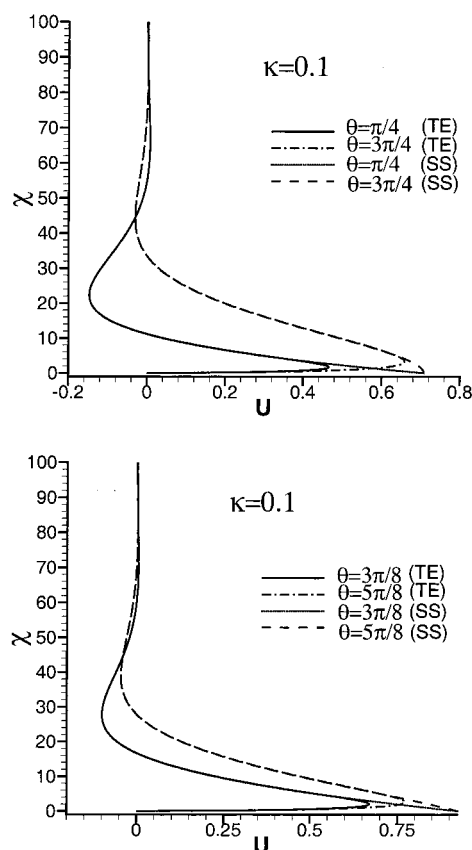

Figure 4. Comparisons between the time-periodic electroosmotic velocity (TE) and the Stokes' second problem (SS) for $\kappa = 0.1$ at various instances in time. The results are obtained for ionic energy parameter $\alpha = 5.0$. Top panel shows times $\pi/4$ and $3\pi/4$, and the bottom panel shows times $3\pi/8$ and $5\pi/8$.

velocity field and shows fluid rotation. From the $\kappa = 0.01$ and $\kappa = 0.1$ cases, we see that the time-periodic electroosmotic flows *are not irrotational*, when the diffusion length scale is comparable to or less than the channel half-height ($l_D \leq h$). The vorticity is put into the problem on the walls, and its magnitude alternates by time due to the time fluctuations of the external electric field. Unlike the steady electroosmotic flows, the vorticity diffuses deeper into the channel, while its value on the wall is cyclically changing. The high-frequency excitation case ($\kappa = 0.1$) presented in Figure 3 shows exponentially damped vorticity waves traveling into the bulk flow domain, penetrating the channels as much as 80 Debye lengths. A discussion on vorticity creation mechanisms for unsteady electroosmotic flows is given by Santiago.[18] Our results further validate these findings.

The velocity profiles presented in Figure 3 resemble the classical solution of flat plate oscillating in a semi-infinite flow domain, also known as the Stokes' second problem. In Figure 4, we compare the time periodic electroosmotic velocity profiles against the solution of Stokes' second problem. Unlike the time periodic electroosmotic flow, the fluid is driven here by an oscillating plate with a velocity $u_w = u_{HS} \mathrm{Sin}(t\Omega)$, where Ω is the frequency of the plate oscillations and u_{HS} is the amplitude of the plate velocity. The governing equation for Stokes' second problem becomes

$$\rho_f \frac{\partial u}{\partial t} = \mu \frac{\partial^2 u}{\partial y^2} \tag{18}$$

and the system is subjected to the following boundary conditions:

$$u(y = 0, t) = u_{HS} \mathrm{Sin}(t\Omega)$$

$$u(y \rightarrow \infty, t) = 0$$

These equations yield the following similarity solution:[19]

$$U(\chi, \theta) = \exp\left[-\frac{\kappa\chi}{\sqrt{2}}\right] \mathrm{Sin}\left[\theta - \frac{\kappa\chi}{\sqrt{2}}\right] \tag{19}$$

where U is the velocity normalized with u_{HS}, similar to our solution of time-periodic electroosmotic flow. The solutions for both

equations are practically the same for $\chi \geq \delta_{99}$ (See Figure 4). Therefore, the bulk flow dynamics is adequately described by the Stokes' solution for a flat plate oscillating with frequency Ω and amplitude u_{HS}. However, the velocity distribution within the effective electric double layer ($\chi \leq \delta_{99}$) differs from the Stokes' solution significantly, as the velocity on the wall needs to obey the no-slip condition at all times. A zoomed view of the velocity distribution of Figure 4 is presented in Figure 5.

In numerical modeling of electroosmotic flows, resolution of the EDL region creates a numerical stiffness, requiring increased grid resolution. Therefore, it is important to develop appropriate velocity slip models that allow accurate representation of the bulk flow region without a general loss of accuracy. Matching between the Stokes' solution and our analytical solution outside the effective EDL thickness (without any phase lag) enables us to conclude that Stokes' solution with a prescribed wall velocity of $u_{HS} \mathrm{Sin}(t\Omega)$ can be used to describe the bulk flow region for sufficiently large κ values. This shows that the *instantaneous* Helmholtz−Smoluchowski velocity is the *appropriate slip condition* for time-periodic electroosmotic flows. Here we must note that this claim is also valid for low-frequency (small κ) flows as can be deduced from Figure 2 by extending the velocity profiles from the bulk flow region on to the wall. Figure 5 also shows significant differences between the instantaneous velocity magnitude at the

(18) Santiago, J. G. *Anal. Chem.* **2001**, *73*, 2353−2365.
(19) Panton, R. L. *Incompressible Fluid Flow*; Wiley: New York, 1984.
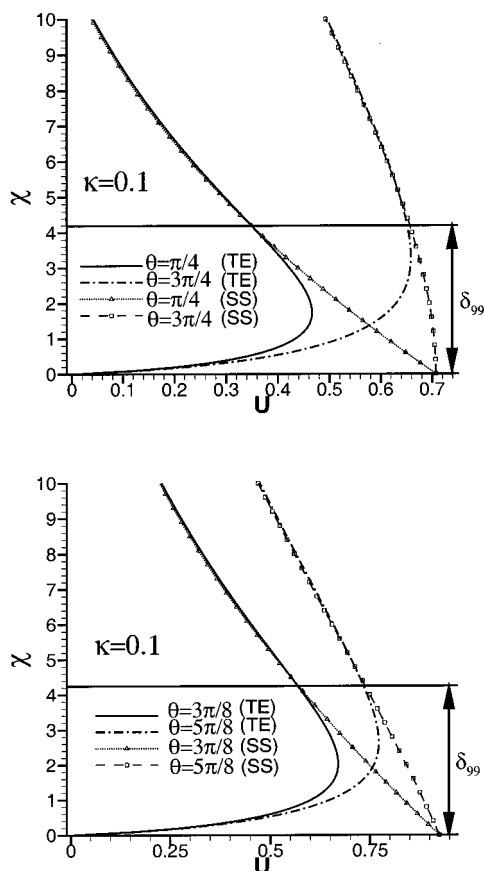
Figure 5. Near-wall velocity distribution for time-periodic electroosmotic flow and Stokes' second problem for $\kappa = 0.1$ at various times. See the caption for Figure 4 for the details.

Figure 6. First derivative of the velocity in the cross-flow direction as a function of χ. This figure also corresponds to negative of the fluid vorticity.

edge of the EDL (at $\chi = \delta_{99}$) and $u_{HS} \sin(t\Omega)$ on the walls, which indicates that the instantaneous value of Helmholtz−Smoluchowski velocity *cannot be used as the velocity matching condition at the edge of the EDL*. This result is in agreement with our previous findings.[14]

An interesting aspect of our analytical solution is that unlike the Stokes' solution the velocity profiles in our solution have to match the no-slip condition on the walls at all times. This creates *inflection points* in the velocity distribution very near the walls. The first derivatives of the velocity profiles are presented in Figure 6 for $\kappa = 0.1$ at different times, obtained via a second-order finite differencing technique. Since we differentiated the streamwise velocity component in the normal direction to the channel walls, the first derivative of the velocity here also corresponds to the negative of the fluid vorticity ($-\partial U/\partial\chi$). From Figure 6, we see that $dU/d\chi$ has a local minimum ($d^2U/d\chi^2 = 0$) around $3 \leq \chi \leq 15$ (depending on the time instant), which corresponds to *inflection points in the velocity profile*. The presence of inflection points with vorticity extrema *may* result in flow instabilities. At this moment, we have not performed a stability analysis of our analytical solution. However, our results can be used to develop a series of well-planned experiments, systematically exploring low Reynolds number flow instabilities.

SUMMARY AND CONCLUSIONS

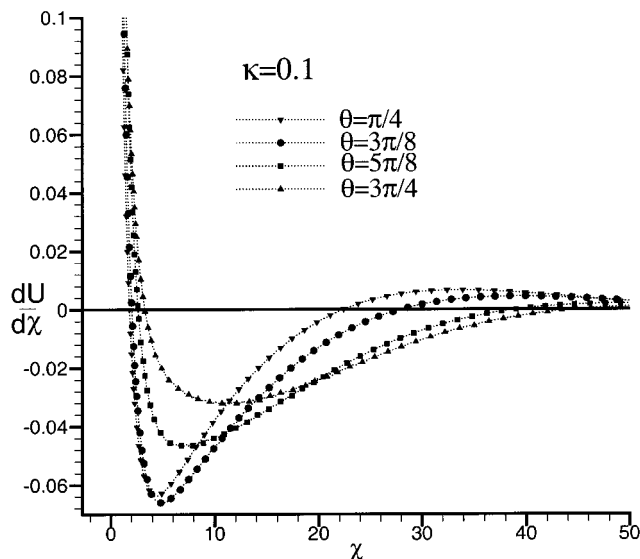We obtained an analytical solution for time-periodic electroosmotic flows in two-dimensional straight microchannels by assum-ing a constant ζ potential, constant buffer concentration, and Newtonian fluid. Our analysis has resulted in the following:

The flow dynamics is determined by a normalized parameter κ, which can be interpreted as the ratio of the EDL thickness to a characteristic diffusion length scale l_D. On the basis of the values of κ and the half channel height, various flow conditions, ranging from the quasi-steady oscillatory plug flow to flows resembling the flat plate oscillating in a semi-infinite domain with velocity u_{HS} $\sin(t\Omega)$ (Stokes' second problem) are observed.

For large values of κ, we identified similarities between the Stokes' second solution and our analytical solution in the bulk flow region. This led to identification of the instantaneous Helmholtz−Smoluchowski velocity as the appropriate electroosmotic slip condition for time-periodic flows.

We have found that the bulk flow region may become *rotational* for sufficiently large values of κ. The vorticity is put into the problem on the walls, and its magnitude alternates by time due to the time fluctuations of the external electric field. Unlike the steady electroosmotic flows, the vorticity diffuses deeper into the channel, while its value on the wall is cyclically changing. For large κ values, this creates exponentially damped vorticity waves traveling into the bulk flow region, similar to the Stokes layers.

Analytical solution of the velocity profiles shows near-wall inflection points with localized vorticity extrema. The location of the first inflection point near the wall and its vorticity magnitude are significantly different from the Stokes layers. We expect this to affect the stability characteristics of time periodic electroosmotic flows.